Boundaries, kinetic properties, and final domain structure of plane discrete uniform Poisson-Voronoi tessellations with von Neumann neighborhoods

A. Korobov*

Materials Chemistry Department, V. N. Karazin Kharkov National University, Kharkov 61077, Ukraine

(Received 10 April 2008; revised manuscript received 18 January 2009; published 24 March 2009)

Discrete random tessellations appear not infrequently in describing nucleation and growth transformations. Generally, several non-Euclidean metrics are possible in this case. Previously [A. Korobov, Phys. Rev. B **76**, 085430 (2007)] continual analogs of such tessellations have been studied. Here one of the simplest discrete varieties of the Kolmogorov-Johnson-Mehl-Avrami model, namely, the model with von Neumann neighborhoods, has been examined *per se*, i.e., without continualization. The tessellation is uniform in the sense that domain boundaries consist of tiles. Similarities and distinctions between discrete and continual models are discussed.

DOI: 10.1103/PhysRevE.79.031607 PACS number(s): 81.15.Aa, 05.20.Dd

I. INTRODUCTION

Apparently simple Kolmogorov-Johnson-Mehl-Avrami (KJMA) theory [1–3] proves to be extensively exploitable over decades in ever growing number of fields. Historically starting from steel crystallization [1–4], it is currently employed in describing such disparate at first glance processes as DNA replication [5,6] and phase separation in multicomponent alloys [7], biosorption in living cells [8] and solid state reaction kinetics [9,10], cryopreservation of biological tissues [11] and film growth on solid substrates [12], etc. This inspires continuous theoretical efforts in developing the theory and in extending it beyond fairly strong applicability conditions explicitly stated in [1]. In many of these works the KJMA theory serves as the starting point and comparison standard. Recent extensions of the theory include, in particular, the account of finite volume [13], nonrandom nucleation, and overgrowth processes [14], anisotropic growth [15], continuous heating conditions [16], screening effects [17]. In the framework of the KJMA theory the explicit solution has been found for the temporal evolution of the domain structure in the Poisson-Voronoi case for arbitrary dimension [18–20]. Also, the sidedness probability has been studied in detail for this type of tessellations using Monte Carlo (MC) method [21]. One more recent result is the statistical properties in the case of time-dependent nucleation and growth rates with no imposed restrictions [22]. In all cases the Euclidean metric is implied.

This paper presents a simple discrete two-dimensional (2D) version of the KJMA model on the square tiling. Both nucleation and growth are discrete. Discrete nucleation means that a nucleus possesses definite size and cannot be considered as a point. Nucleation on the tiling is simultaneous and spatially almost random; with a small correction required to provide uniform domain boundaries as described below. Discrete growth means that at each step s standing for discrete time all adjacent tiles join the growing nucleus. Linear growth is considered, and accordingly the ultimate tessellation is a discrete analog of conventional Poisson-Voronoi tessellations. In topological respect, a peculiarity is the finite number of growth directions, whereas in continual 2D nucleation-growth models this number is infinite (but is finite in 1D continual case). In metrical respect, a peculiarity is that the discrete growth mode determines the metric different from the Euclidean metric. Two basic modes are possible on a square tiling determined by the von Neumann and Moore neighborhoods. Note that both of them have been recently considered in [23] (with subsequent continualization) in studying the anisotropic growth. This paper deals with the former. Compared to lattice models, e.g., semideterministic lattice models [24], two main distinctions are non-Euclidean metric and definite dimensions of tiles.

To compare a discrete model with the conventional KJMA theory it needs to be continualized since there is no natural discretization for the Euclidean metric. This was done in [25]. The free boundary length as a function of the nucleus radius was shown to be sensitive to the metric, whereas the final area distribution is practically invariant. But in passing to continual analogs, some peculiarities of discrete tessellations are obviously lost. With this in mind, this paper examines the discrete tessellation *per se* to reveal distinctions and similarities with continual analogs. The main emphasis is on the kinetic properties and final area distributions. A necessary attention is also paid to peculiarities of domain boundaries.

II. TESSELLATION

This section describes the model tessellation under study. One square tile is considered as the nucleus capable of subsequent stable growth. This is a typical zero approximation. In the present context the oversimplification is not too strong: presented results can be generalized for more involved cases of nucleation. Some aspects of the transformation of random irregular nuclei into regular islands with the same form and orientation are discussed in [26]. All nuclei appear simultaneously at the very beginning of the growth process; no additional nuclei appear during the growth process. Nuclei are randomly distributed on the square tiling, but further undergo a small correction as explained below.

*Alexander.I.Korobov@univer.kharkov.ua

 ©2009 The American Physical Society

The growth process is irreversible, discrete, and symmetrical: at each step s (standing for discrete time) the interface propagates to all symmetrically equivalent tiles adjacent with a growing island. On the square tiling two growth modes correspond to these conditions (Fig. 1): (a) a tile joins the growing island only if they have a common edge; (b) a tile joins the growing island if they have a common vertex. In the first case $4s$ tiles are joined at step s; in the second case the number of joining tiles is $8s$. These modes may be described in terms of the displacement vectors. The first case is termed von Neumann neighborhood; the displacement vector is

$$N_5 = \left\{ \begin{pmatrix} 0 \\ 0 \end{pmatrix}; \quad \begin{pmatrix} 1 \\ 0 \end{pmatrix}; \quad \begin{pmatrix} 0 \\ 1 \end{pmatrix}; \quad \begin{pmatrix} -1 \\ 0 \end{pmatrix}; \quad \begin{pmatrix} 0 \\ -1 \end{pmatrix} \right\}. \quad (1)$$

The second case is termed Moore neighborhood; the displacement vector is

$$N_9 = \left\{ \begin{pmatrix} 0 \\ 0 \end{pmatrix}; \begin{pmatrix} 1 \\ 0 \end{pmatrix}; \begin{pmatrix} 0 \\ 1 \end{pmatrix}; \begin{pmatrix} -1 \\ 0 \end{pmatrix}; \begin{pmatrix} 0 \\ -1 \end{pmatrix}; \begin{pmatrix} 1 \\ -1 \end{pmatrix}; \begin{pmatrix} -1 \\ 1 \end{pmatrix}; \begin{pmatrix} 1 \\ 1 \end{pmatrix}; \begin{pmatrix} -1 \\ -1 \end{pmatrix} \right\}. \quad (2)$$

The distance between two nuclei is defined as the number of tiles in the shortest chain of tiles connecting nuclei. As illustrated in Fig. 1, thus defined distance is different for different growth modes; for the same mutual situation of nuclei the distance is nine in the first case (c) and is five in the second case (d). Generally, for von Neumann neighborhood the distance is

$$D_N = |\Delta x| + |\Delta y|. \quad (3)$$

For Moore neighborhood it reads

$$D_M = \max(|x - x_0|, |y - y_0|) \quad (4)$$

In this way the growth mode determines the metric.

Islands are fixed and grow to impingement. Upon impingement the growth in the direction of impingement is stopped; in other directions it proceeds according to the above rules. Note that the number of directions in the discrete case is finite in contrast to 2D continual models. Ultimately this results in a random discrete tessellation.

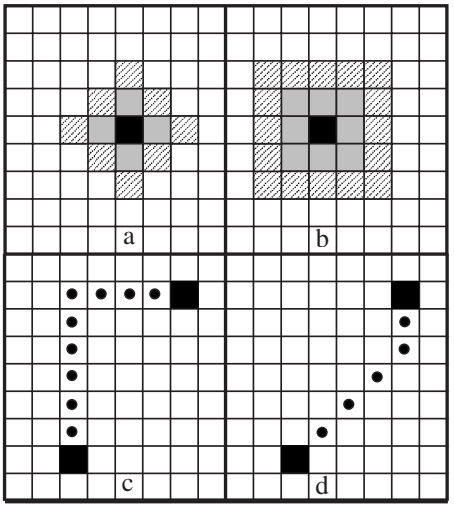

FIG. 1. Two growth modes on the square tiling: von Neumann neighborhood (a) and Moore neighborhood (b). They determine different distances between two nuclei, (c) and (d), respectively.

Tessellations with von Neumann neighborhood are selected to start with. On the one hand, this is the simplest case. On the other hand, the island is intermediate between compact and ramified shapes, and various scenarios may be further considered.

In studying discrete tessellations one faces a number of peculiarities which have no analogs in the conventional continual case. The first peculiarity is the structure of boundaries, which needs to be addressed in some detail to make possible the study of various properties.

III. BOUNDARIES

In constructing a conventional continuous tessellation, the random Voronoi cell is defined as the geometric locus, points of which are closer to a particular nucleus than to any other nucleus. Voronoi cells fill the whole space without overlaps. Boundaries in this case have zero measure and fairly simple structure: each boundary point is equidistant from two nuclei except vertexes which are equidistant from three nuclei. It is logical to construct a discrete analog in the same manner: tiles are allotted to nearest nuclei in the corresponding metric, and each random domain consists of tiles which are closer to a particular nucleation tile than to any other nucleation tile. The problem is that boundaries in the discrete case appear to be more involved.

Figure 2 shows that boundaries may be either lines or chains of tiles depending on the distance between nuclei. We remind the reader that the distance between two nuclei is the number of tiles in the shortest chain connecting these nuclei (nucleation tiles are not included). If the distance is even, the boundary is the line (e.g., the boundary between nuclei b and c in Fig. 2); if the distance is odd, the boundary is the chain of tiles (e.g., the boundary between nuclei a and b in Fig. 2).

Generally, discrete random tessellations have mixed boundaries. It is impossible to construct a tessellation with only linear boundaries. But it is possible to construct a tessellation with only tiling boundaries. To do this, the square

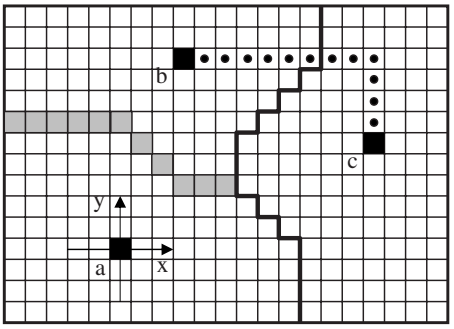

FIG. 2. Two types of boundaries, linear and tiling; solid circles show the distance between nuclei b and c.

tiling is considered as a big chessboard. First, nuclei are placed at random at all the tiles. Then each nucleation tile that turns out to be black is shifted at random to one of nearest white tiles (or vice versa). This is a slight violation of the initial randomness. Tessellations of this type will be termed tessellations with uniform boundaries or, briefly, uniform tessellations. An example is shown in Fig. 3. Square tiles fall into nuclei (nucleation tiles), boundary tiles and interior tiles of random domains (Voronoi domains). In this paper only uniform tessellations will be considered as the simplest case.

Note that boundaries in this case have nonzero measure. To ensure that the whole space will be filled after a nucleation and growth process is completed, the impingement of two nuclei is defined as the event when these nuclei occupy the nearest equidistant boundary tile. In calculating domain areas, this tile is equally divided between two domains. Accordingly, the area of a random domain is the sum of areas of all interior tiles plus one half of areas of boundary tiles equidistant from two nuclei plus one third of areas of boundary tiles equidistant from three nuclei, etc. The sum of all domain areas equals to the area of the whole space. No changes are required if one wants to pass to tessellations with mixed boundaries. Thus, this paper deals with discrete random Poisson-Voronoi tessellations with square tiles, one-tile stable nuclei, von Neumann neighborhoods, and uniform boundaries. Corresponding metric (3) will be termed Q_N metric.

The boundary between two nuclei has a definite structure (Fig. 2):

(i) The number of tiles in its stepwise part is equal to $\min(|\Delta x|,|\Delta y|)+1$.

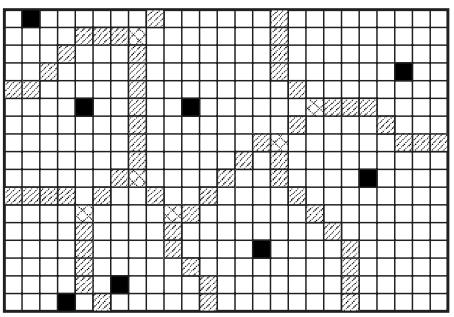

FIG. 3. An example of discrete random tessellation; the double hatching denotes vertices.

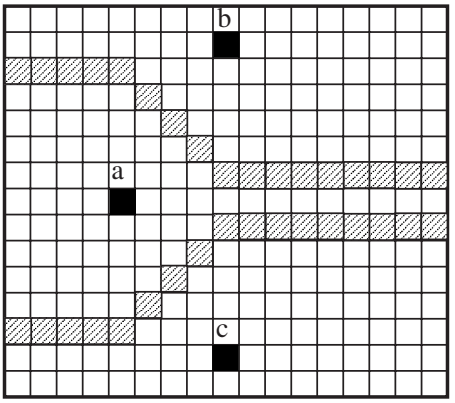

FIG. 4. Three nuclei may have no equidistant tile; nuclei b and c are not adjacent.

(ii) If the origin of coordinates is associated with one of nucleation tiles (nucleus a in Fig. 2), one of the above boundary tiles is surely situated on one of these axes (axis y in Fig. 2).

(iii) The stepwise part may be prolonged (*ad infinitum* if there are only two nuclei) in both directions by straight parts oriented along the second axis.

(iv) The stepwise part may consist of only one tile; in this case one obtains simply a straight boundary parallel to one of the axes.

On the Euclidean plane three points (not on one line) determine a circle with the center equidistant from these three points. This is used, in particular, in constructing random tessellations [27]. In the Q_N metric this is not always the case. Figure 4 illustrates the situation when three nuclei have no common vertex; nuclei b and c are not adjacent.

As was mentioned above, boundaries of conventional tessellations contain points equidistant from two or three nuclei; there are no other possibilities. Boundaries of discrete tessellations are more involved in this respect. They include tiles equidistant from four, five, etc., nuclei. For brevity this will be termed the multiplicity μ of a boundary tile. Multiplicity twelve was observed for tessellations with high density of nuclei. Note that the multiplicity is defined as the number of nuclei equidistant from the given boundary tile. For vertices this is not obligatory coincide with the number of outgoing edges. Thus, in Fig. 5 there are two fourfold vertices, B and C. The former has four outgoing edges formed by twofold tiles; the latter has three outgoing edges formed by threefold tiles. An edge can join vertices with different multiplicity;

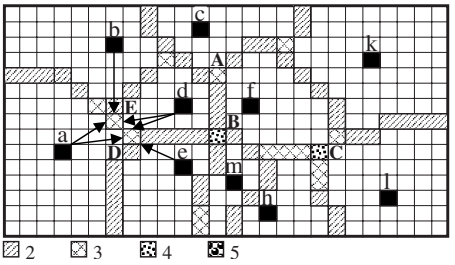

FIG. 5. Examples of boundary tiles with various multiplicities.

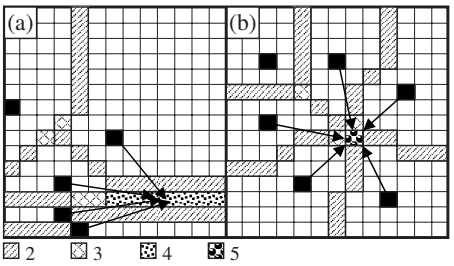

FIG. 6. Examples of boundary structures.

e.g., edge AB joins threefold vertex A and fourfold vertex B. An edge may include tiles with various multiplicities; e.g., the edge joining vertices B and C consists partly of twofold and partly of threefold tiles. Two vertices may be immediate neighbors with no edge between them; e.g., vertices D and E in Fig. 5. Vertex D is formed by nuclei a, d, and e; vertex E is formed by nuclei a, b, and d; there is no edge between them.

A further peculiarity is that boundary tiles may form two-dimensional arrays. An example is given in Fig. 6(a). Four nuclei form a boundary consisting of fourfold tiles. From above and below they border with twofold boundary tiles. Also, this array includes two threefold tiles. On the other hand, the presence of a vertex with high multiplicity is not necessarily associated with involved two-dimensional arrays of boundary tiles. Figure 6(b) shows a fragment of random tessellation which has a fivefold vertex and one-dimensional boundaries consisted mainly of twofold tiles.

IV. PROPERTIES

Kinetics of the interface length is of the main interest in this section since this characteristic was shown to be sensitive to the metric in continualized cases. Kinetics is studied not only for the whole tessellations (with different density of nuclei) but also for subsets of random Voronoi domains with 4, 5, etc., neighbors. Accordingly, computation of necessary statistics precedes the study of kinetic properties. Area distributions are also studied in connection with kinetics: results obtained support the mutual situation of kinetic curves. In addition, distances to neighbors are computed and compared with distances in the Euclidean metric.

A. Distribution of domains in the number of neighbors

One of the most general and long-known properties of conventional random tessellations is the number of edges of the typical cell which is always six [28,29]. In other words, nucleus has six neighbors in the average. Naturally, the first step is to examine this property in our discrete case.

Uniform discrete tessellations are convenient in computational respect. A tessellation is represented as the three-dimensional array $A(d1\times d2\times 15)$; $d1$ and $d2$ determine the size of the tiling; the third dimension is used for storing characteristics of each tile. The density of nuclei Λ is defined as the ratio of the number of nuclei N to the total number of tiles in the tiling; $\Lambda=N/(d1\times d2)$. In all computations N was 10 000. Positions of nuclei were selected at random and corrected at random as described above to be only odd to provide the uniformity of the generated tessellation. All results discussed below are the average of 25 simulations.

TABLE I. The ratio of interior and boundary tiles with the account of multiplicity.

		Nuclei density Λ			
		0.0001	0.001	0.01	0.1
Maximum step		362	85	30	10
Maximum multiplicity		5	6	7	12
Percentage of interior tiles		97.6	91.9	77.8	41.7
Percentage of boundary tiles					
	Total	2.4	8.0	21.4	49.3
With multiplicity	2	2.3	7.4	17.4	27.0
	3	0.05	0.5	3.2	13.4
	4	10^{3}	0.03	0.5	5.7
	5	10^{-5}	10^{-3}	0.08	2.2
	6	—	10^{-4}	0.01	0.8
	7	—	—	10^{-3}	0.3
	8	—	—	—	0.05

With the account of the above peculiarities, boundaries were determined in the following way. For each tile of the tessellation distances were computed in the Q_N metric to all nucleation tiles and the minimal distance was identified. Then the number of these minimal values in the array of distances was determined. This is the multiplicity of a tile μ (the numbers of equidistant nuclei). It was stored in the array A for further computations. Also, the step number s at which a given tile is reached by a growing nucleus was computed.

To avoid boundary effects, all boundary random domains, i.e., domains bordered partly by boundary tiles and partly by the border of initial tiling, have been rejected. The resulting piece of tiling has an irregular shape and is completely bordered with boundary tiles at which the growth process vanishes. No one nucleus can grow beyond these boundaries, and all tiles will be ultimately captured by the growth process.

Two nuclei are neighbors if they have at least two common boundary tiles irrespectively of their multiplicity. If they have only one common boundary tile (vertex) they are not neighbors.

The range of Λ studied was 0.1 to 0.0001. Obviously, Λ must be less than unity: $\Lambda=1$ would mean that each tile is the nucleation tile. In the case of dense tessellations the percentage of boundary tiles is fairly big and the growth process takes relatively few steps. Thus, for $\Lambda=0.1$ half of all tiles are boundary tiles and the growth process is completed in only 10 steps (Table I). Several tiles with multiplicities 9 to 12 have been observed (not reflected in the table). With the decrease of Λ the percentage of boundary tiles and the maximal multiplicity decrease while the number of steps increases. The study of sparse tessellations is computationally more demanding.

TABLE II. Distribution of random domains in the number of immediate neighbors.

Number of neighbors ν	Percentage of tiles with ν neighbors				
	$\Lambda=0.1$	$\Lambda=0.01$	$\Lambda=0.001$	$\Lambda=0.0001$	Conventional tessellation [30] $\lambda=0.93$
3	—	—	—	—	2
4	1.4	**5.3**	9.4	12.3	13
5	13.1	**17.6**	22.9	25.8	24
6	24.4	**26.5**	**27.6**	**27.9**	**28**
7	**25.3**	**23.3**	21.4	19.8	21
8	18.5	**15.3**	11.9	8.9	8
9	10.1	**7.4**	4.6	3.2	2
10	4.6	**2.9**	1.5	1.3	1

The distributions of random domains in the number of immediate neighbors ν are shown in Table II. Domains with six neighbors prevail in all tessellations except the densest one, in which domains with seven neighbors dominate. With the decrease of Λ the percentage of domains with ν equals 4 to 6 increases whereas the percentage of domains with the coordination numbers 7 and greater decreases. Generally, distributions tend to that for continual random Voronoi tessellation with $\lambda \approx 1$ (last column of Table II); λ is the density of nuclei in the continuous case. The main distinction is that no random domains with three neighbors were registered for discrete tessellations. More than 97% of all random domains have 4 to 10 immediate neighbors.

B. Kinetics

Now it is possible to study the KJMA kinetics of discrete tessellations. This is done in the way described in [25]. Briefly, the growth of each island inside its random domain is followed in dynamics starting from the moment of nucleation and up to the moment when the domain is completely filled; boundary tiles are equally divided between all equidistant nuclei according to their multiplicity as described above. Kinetic curves for discrete tessellations have been computed in the following way. Function $n(s)$ was associated with each random domain of a tessellation, where n is the number of tiles actually joined the island at step s (in other words, actual interface length expressed as the number of interface tiles). This curve is termed primitive kinetic curve. An example is shown in the insert of Fig. 7. The sum of all primitive curves normalized on the total number of nuclei gives the kinetic curve $N(s)$ which characterizes kinetic properties of the random tessellation as a whole [solid lines in Figs. 7(a) and 7(b)]. In the case of $\Lambda=0.1$ curves are not smooth because of fairly small number of steps required to complete the growth process. As was shown in [25], in the continual case corresponding kinetic curves are not scaled into similar curves computed in the Euclidean metric.

In the conventional continuous case domains with six neighbors have been shown to be representative in kinetic respect [30]. To examine this regularity in the discrete case, kinetic curves $N_\nu(s)$ were computed separately for random domains with 4, 5, 6, 7, 8, and 9 neighbors as sums of corresponding primitive curves normalized on the number of domains with ν neighbors. Results for $\Lambda=0.0001$ and $\Lambda=0.1$ are shown in Fig. 7. In all four studied cases the tendency is the same as was previously observed for conventional Voronoi tessellations with the Euclidean metric: with the increase of ν the maximum is shifted upwards and right. This agrees with the area distribution described below. $N_6(s)$ curve provides a reasonably good approximation to $N(s)$ curve in the case of $\Lambda=0.0001$. Note that in this case the percentage of domains with six neighbors is the biggest (Table II). On the contrary, for $\Lambda=0.1$ $N(s)$ curve practically coincide with $N_7(s)$ curve. The prevalence of domains with

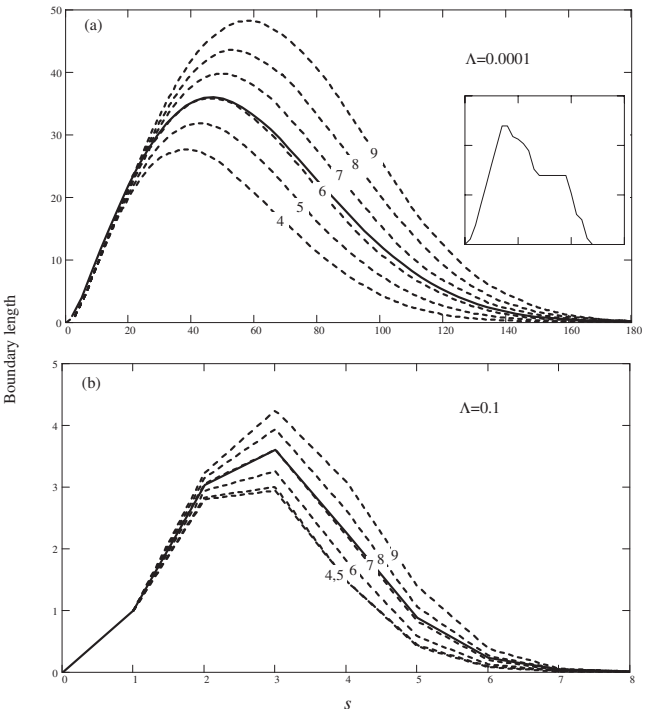

FIG. 7. Kinetic curves for the whole tessellation (solid) and for separate subsets of domains with ν neighbors (dashed); an example of primitive kinetic curve is shown in the inset.

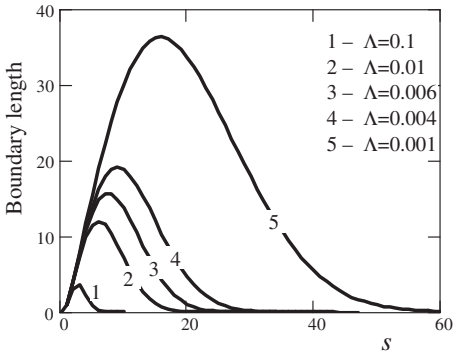

FIG. 8. Kinetic curves of tessellations with different density of nuclei Λ.

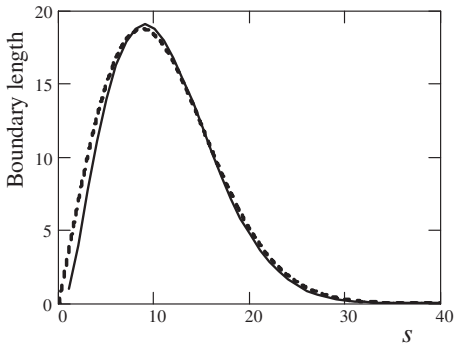

FIG. 9. Numerical kinetic curve for discrete tessellation (solid) in comparison with scaled analytical curve for continual tessellation (dashed); Λ=λ=0.004.

$\nu=7$ over domains with $\nu=6$ is only 1%, but domains with $\nu=8$ considerably prevail over domains with $\nu=5$, while in the case of $\Lambda=0.0001$ the ratio is inverse. For other values of Λ $N(s)$ curves are situated between $N_6(s)$ and $N_7(s)$ curves. Generally, with the increase of Λ the maximum of $N(s)$ curves is shifted left and downwards (Fig. 8). In the case of $\Lambda=0.0001$ (not shown in Fig. 8) $s=50$, $N(s)=114$.

Discrete results may also be compared with analytical results obtained for the metric under study in the framework of the KJMA approach [25]. The analytical expression for the boundary length L as a function of radius r (proportional to time) reads

$$L(r) = 4\sqrt{2}r\exp(-2r^2\lambda). \tag{5}$$

(Note that in [25] L is given per unit area.) For comparing discrete and continual results it is reasonable to take the edge of the tile as the unit length. Then $\lambda=\Lambda$. Positions of maxima on kinetic curves corresponding to different Λ are compared in Table III. Taking into account that values of s are integer, $r_{\max}$ and $s_{\max}$ agree well except the densest tessellation. $L_{\max}$ and $N_{\max}$ differ, but their ratio $\eta=N_{\max}/L_{\max}$ is practically the same for all values of Λ, about 0.7 (Table III). Using this value, $L(r)$ curves may be scaled into $N(s)$ curves when $r_{\max}$ and $s_{\max}$ are close enough,

$$N(r) = \eta L(r). \tag{6}$$

The result of scaling in the case of $\Lambda=0.004$ is shown in Fig. 9 as an example; for smaller values of Λ fitting is similar. But for $\Lambda=0.1$ scaling is obviously impossible since $r_{\max}$ and $s_{\max}$ differ considerably. The value of η is connected in some way with the discrete nature of the growth process. Note also that the KJMA approach requires the convex shape of growing islands. Discrete islands with von Neumann neighborhood are not convex.

TABLE III. Positions of maxima on kinetic curves in discrete and continual cases.

Nuclei density $\lambda=\Lambda$	Continual model; Eq. (5)		Discrete model; Fig. 7		
	$r_{\max}$	$L_{\max}$	$s_{\max}$	$N_{\max}$	η
0.001	15.8	54	16	36	0.66
0.004	7.9	27.5	9	19	0.69
0.006	6.5	21.7	7	16	0.74
0.01	5.0	17	6	12	0.71
0.1	1.58	5.4	3	4	0.74

C. Area distributions

To obtain a deeper insight into the above results they need to be related to the distribution of domain areas. The transformation is believed to be completed, and the area of a random domain is just the number of tiles belonging to this domain. The nucleation tile is included and boundary tiles are equally divided between nuclei from which they are equidistant. Thus computed areas S have been scaled as $S/\bar{S}$ (where the mean area $\bar{S}=1/\Lambda$) and the histogram constructed from these data have been normalized to unit area. Results for various Λ are shown in Fig. 10. Solid lines correspond to the commonly used Kiang conjecture [31]

$$F(y) = \frac{c^c}{\Gamma(c)} y^{c-1}\exp(-cy), \tag{7}$$

where y is the scaled area. This conjecture works in all cases. Analytically derived value of the parameter c in the conven-

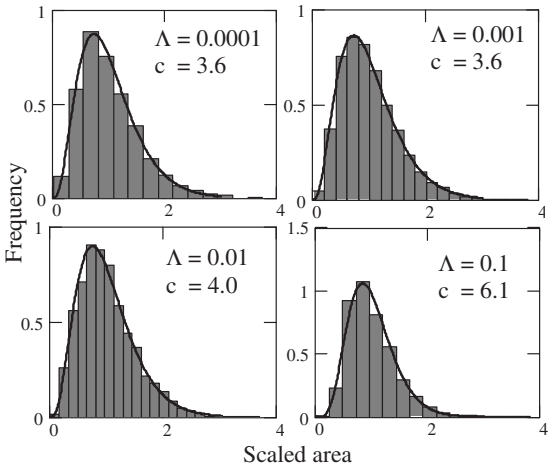

FIG. 10. Area distributions of random domains (histogram) in comparison with the Kiang conjecture (solid line) for different nuclei density.

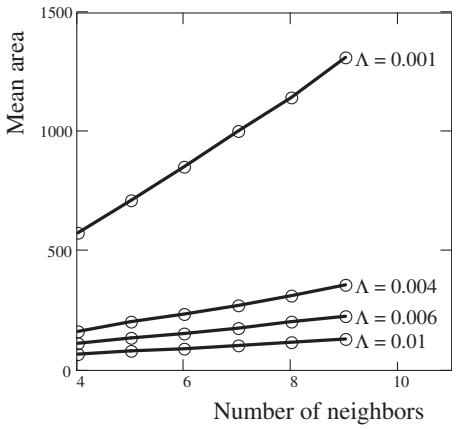

FIG. 11. Mean area computed for subsets of random domains with various numbers of immediate neighbors.

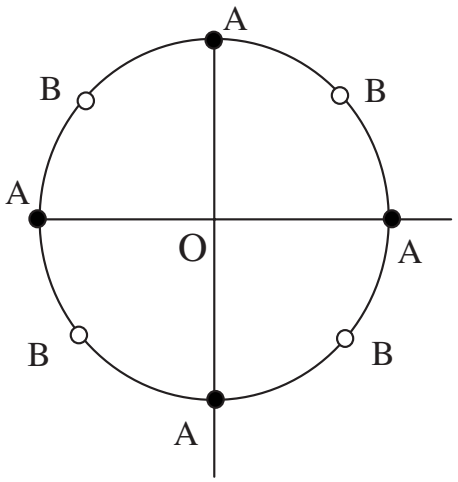

FIG. 12. For points A distances from O is the same in both metrics Q_N and E; for points B the difference of distances is the biggest.

tional continual case equals 3.575 [32]. This value provides good fitting for scares discrete tessellations, but in passing to denser tessellations it considerably increases. The invariance of the area distribution with respect to the metric in the continual case has been shown previously [25], and it is reasonable to suppose that the increase of c is a consequence of the high percentage of boundary tiles.

An interesting and somewhat unexpected result is the linear dependence of the mean area S_ν computed separately for subsets of random domains with ν immediate neighbors on ν (Fig. 11). Only four lines are shown because it is impossible to combine all results in one figure. But linearity is observed for all studied values of Λ. Slopes are 1.2, 14.1, 23.1, 39.5, 147.9, and 1490 for Λ 0.1, 0.01, 0.006, 0.004, 0.001, and 0.0001, respectively. This agrees with the mutual situation of kinetic curves in Fig. 7. Intuitively clear that the mean area must decrease at higher ν. But $\nu > 10$ is a fairly rear event, and in the present study no statistically significant results have been obtained. Fragmentary observations show that the mean area tends to increase up to $\nu=12$, though not so rapidly.

In Table IV the mean areas computed for subsets of random domains with six and seven immediate neighbors are compared with mean areas of the whole tessellations with different Λ. In the case of the most scares tessellation the subset of domains with $\nu=6$ represents well this characteristic: the discrepancy is only 2%. In the most dense tessellation domains with $\nu=7$ are representative in this respect. This is in agreement with kinetic characteristics discussed above.

D. Distances to neighbors

Finally, the averaged distances to the nearest, second, etc., neighbors have been computed for all tessellations to compare with corresponding distances in the Euclidian metric (E). Only results for $\Lambda=0.004$ are shown in Table V as an example. Since there is no natural discretization for the Euclidean metric, distances have been computed between centers of nucleation tiles and the side of the tile has been taken as the unit length. $\chi=\delta_Q(a,b)/\delta_E(a,b)$ is the ratio of averaged distances computed in both metrics.

TABLE IV. Deviation (%) of S_ν from S for different Λ.

	Nuclei density Λ			
ν	0.1	0.01	0.001	0.0001
6	12	10	5	2
7	1	3	11	17

Computations revealed the constancy of the averaged value of χ irrespectively of Λ; for all values of Λ it falls within the range 1.25–1.27. This may be explained as illustrated in Fig. 12. Points of the circle are equidistant from point O in the E metric. In the Q_N metric their distances from O vary in the range $(R, R\sqrt{2})$, where R is the circle radius (in E metric). Only four points (A) have the same distances in both metrics. There are four points (B) for which the difference of distances is the biggest. The rest of points are intermediate in this respect. For symmetry considerations it is reasonable to estimate χ as $\frac{1}{\pi/4}\int_0^{\pi/4}(\sin\theta+\cos\theta)d\theta \approx 1.27$, which is in the good agreement with the above empirical results. Averaged distances to neighbors in the Euclidean metric can be calculated analytically exploiting the rigorously proved relationship [33]

$$\langle \delta_k \rangle = \frac{\Gamma(k+1/2)}{(k-1)!\sqrt{\pi\lambda}}, \tag{8}$$

where k is the number of the neighbor, $\Gamma(x)$ is the Euler function, λ is the density of nuclei. Now relationship (8) can also be used to estimate averaged distances to neighbors in the Q_N metric exploiting the empirical coefficient χ.

V. SUMMARY

Quite a number of simulations of various 2D nucleation and growth transformations are started on a lattice but later are continualized to obtain analytical relationships. The Euclidean metric is usually implied though sometimes it is poorly agreed with the anisotropy of a problem. In this paper the discrete description is kept up to the end and the metric differs from the Euclidean metric.

TABLE V. Averaged distances to neighbors in Q_N and E metrics; $\Lambda=0.004$.

	Neighbor								
Metric	1	2	3	4	5	6	7	8	9
Q_N	9.86	15.09	19.26	24.01	28.54	32.98	36.49	39.98	41.34
E	7.91	12.01	15.35	19.01	22.58	26.06	29.01	31.67	32.79
χ	**1.25**	**1.26**	**1.26**	**1.26**	**1.26**	**1.27**	**1.26**	**1.26**	**1.26**

One of the simplest possible cases has been examined: square tiles, simultaneous nucleation, one-tile stable nuclei, random distribution of nuclei, von Neumann neighborhood, irreversible growth to impingement, immobile islands. Compared to the continuous analog, the structure of boundaries is much more involved. In spite of different metric, discreteness and square symmetry, the averaged number of neighbors remains six except very dense tessellations with high percentage of boundary tiles. The maximum on kinetic curves is shifted left and downwards with the increase of nuclei density. In sparse tessellations domains with six neighbors are kinetically representative as in the continuous case, but for dense tessellations this is not true. Also, the kinetic curve can be scaled in a simple manner into corresponding analytically calculated curve for continuous tessellation with the same metric if the nuclei density is small; and again this is not the case for dense tessellations. Area distributions of the totally transformed random domains have also been studied. The mean area of domains with definite coordination number increases linearly with the increase of coordination number in the range 4 to 10 at all studied densities. This is in agreement with the mutual situation of kinetic curves for subsets of domains with definite coordination numbers. The Kiang conjecture works well for area distribution in all cases. For sparse tessellations its parameter is close to that for continuous tessellations but with the increase of nuclei density it considerably increases. This emphasizes the nonequivalence of discrete tessellations with different densities in contrast to the universality demonstrated for conventional Poisson-Voronoi tessellations, e.g., in [34,35]. No universal solution for the discrete model follows from the presented results. Further discussion of this interesting subtle point requires similar results for Moore and hexagonal cases.

ACKNOWLEDGMENT

This research was partly supported by the Ukrainian Minister of Education and Science through Grant No. 0104U000663.

[1] A. N. Kolmogorov, Bull. Acad. Sci. USSR **3**, 355 (1937); *Selected Works of A.N. Kolmogorov*, edited by A. N. Shiryayev (Kluwer, Dordrecht, 1992), English translation, Vol. 2, p. 188.
[2] W. A. Johnson and R. F. Mehl, Trans. Am. Inst. Min., Metall. Pet. Eng. **135**, 416 (1939).
[3] M. Avrami, J. Chem. Phys. **7**, 1103 (1939); **8**, 212 (1940).
[4] W. Christian, *The Theory of Transformation in Metals and Alloys* (Pergamon, Oxford, 1975).
[5] S. Jun and J. Bechhoefer, Phys. Rev. E **71**, 011909 (2005).
[6] Scott Cheng-Hsin Yang and J. Bechhoefer, Phys. Rev. E **78**, 041917 (2008).
[7] M. J. Starnik, Int. Mater. Rev. **49**, 191 (2004).
[8] S. N. Dodic, S. D. Popov, and S. L. Markov, Mol. Nutrit. Food Res. **45**, 59 (2001).
[9] A. K. Galwey and M. E. Brown, *Thermal Decomposition of Ionic Solids* (Elsevier, Amsterdam, 1999).
[10] A. Korobov, J. Math. Chem. **24**, 261 (1998).
[11] D. Irimia and J. Karlsson, Biophys. J. **88**, 647 (2005).
[12] M. Fanfoni and M. Tomellini, J. Phys.: Condens. Matter **17**, R571 (2005).
[13] B. A. Berg and S. Dubey, Phys. Rev. Lett. **100**, 165702 (2008).
[14] M. Tomellini and M. Fanfoni, Phys. Rev. B **78**, 014206 (2008).
[15] B. J. Kooi, Phys. Rev. B **73**, 054103 (2006).
[16] J. Farjas and P. Roura, Acta Mater. **54**, 5573 (2006).
[17] A. A. Burbelko, E. Fras, and W. Kapturkiewics, Mater. Sci. Eng., A **413**, 429 (2005).
[18] E. Pineda, V. Garrido, and D. Crespo, Phys. Rev. E **75**, 040107(R) (2007).
[19] E. Pineda and D. Crespo, J. Stat. Mech.: Theory Exp. (2007) P06007.
[20] E. Pineda and D. Crespo, Phys. Rev. E **78**, 021110 (2008).
[21] J. H. Hilhorst, J. Phys. A: Math. Theor. **40**, 2615 (2007).
[22] J. Farjas and P. Roura, Phys. Rev. B **78**, 144101 (2008).
[23] B. J. Kooi, Phys. Rev. B **70**, 224108 (2004).
[24] J. W. Evans, Rev. Mod. Phys. **65**, 1281 (1993).
[25] A. Korobov, Phys. Rev. B **76**, 085430 (2007).
[26] A. Korobov, Complexity **4**, 31 (1999).
[27] J. Møller, *Lectures on Random Voronoi Tesselations*, Lecture Notes in Statistics Vol. 87 (Springer-Verlag, New York, 1994).
[28] J. L. Meijering, Philips Res. Rep. **8**, 270 (1953).
[29] A. Okabe, B. Boots, K. Sugihara, and S. N. Chiu, *Spatial Tessellations: Concepts and Applications of Voronoi Diagrams* (Wiley, Chichester, 2000).
[30] A. Korobov, J. Math. Chem. **25**, 365 (1999).
[31] T. Kiang, Z. Astrophys. **64**, 443 (1966).
[32] E. Pineda, P. Bruna, and D. Crespo, Phys. Rev. E **70**, 066119 (2004).
[33] D. Stoyan, W. S. Kendall, and J. Mecke, *Stochastic Geometry and its Applications* (Akademie-Verlag, Berlin, 1989).
[34] J. D. Axe and Y. Yamada, Phys. Rev. B **34**, 1599 (1986).
[35] J. Farjas and P. Roura, Phys. Rev. B **75**, 184112 (2007).